9. Sieber, W. & Schlickeiser, R. Radio measurements in the fields of gamma-ray sources. I-CG195+04. *Astron. Astrophys.* **113,** 314–323 (1982).
10. Caraveo, P. A. *et al.* An identification for Geminga—A review of all the available data. *Adv. Space Res.* **3,** 77–81 (1984).
11. Spoelstra, T. A. Th. & Hermsen, W. Ratio observations at 21 cm wavelength in the direction of Geminga. *Astron. Astrophys.* **135,** 135–140 (1984).
12. Özel, M. E., Dickel, R. J. & Webber, J. S. Upper limit to any 59.35-s periodic radio emission at 18 cm for mCG195.5+4.5. *Nature* **285,** 645–647 (1980).
13. Seiradakis, J. H. A 928 MHz search for periodicities in 2CG195+O4. *Astron. Astrophys.* **101,** 158 (1981).
14. Manchester, R. N., D'Amico, N. & Tuchy, I. R. A search for short-period pulsars. *Mon. Not. R. Astron. Soc.* **212,** 975–986 (1985).
15. Seiradakis, J. H. *IAU Circ.* No. 5532 (1992).
16. Kuzmin, A. D. & Losovsky, B. Ya. *IAU Circ.* No. 6559 (1997).
17. Shitov, Yu. P. & Pugachev, V. D. Radio pulsar Geminga. Preprint No. 33, Lebedev Physical Inst. (1997).
18. Shabanova, T. Evidence for planet around the pulsar PSR B0329+54. *Astrophys. J.* **453,** 779–782 (1995).
19. Taylor, J. H. & Cordes, J. M. Pulsar distances and the galactic distribution of free electrons. *Astrophys. J.* **411,** 674–680 (1993).
20. Caraveo, P. A. *et al.* Parallax observations with the Hubble Space Telescope yield the distance to Geminga. *Astrophys. J.* **461,** L91–L94 (1996).
21. Izvekova, V. A., Malofeev, V. M. & Shitov, Yu. P. The shapes of mean pulse profiles of pulsars radio emission at the frequency 102.5 MHz. *Astron. Zh.* **66,** 345–354 (1989).
22. Bignami, G. F. & Caraveo, P. A. Geminga: it's phenomenology, it's fraternity, and it's physics. *Annu. Rev. Astron. Astrophys.* **34,** 331–381 (1996).
23. Malofeev, V. M. Pulsar radio spectra. in *Pulsars: Problems and Progress* (eds Johnston, S., Walker, M. A. & Bailes, M.) 271–277 (ASP Conf. Ser. Vol. 105, Astron. Soc. Pacific, San Francisco, 1996).

Acknowledgements. We thank K. Lapaev, S. Tyul'bashev, N. Shchegoleva and T. Shabanova for their help with the observations and the reduction program; W. Sieber, D. Lorimer and I. Malov for discussions and careful reading of the manuscript; and V. Shishov, R. Wielebinski and M. Kramer for discussions and support. This work was supported by INTAS and the Russian RFFI.

Correspondence and requests for materials should be addressed to V.M.M. (e-mail: malofeev@prao.psn.ru).

A single-electron transistor made from a cadmium selenide nanocrystal

David L. Klein*†, Richard Roth†‡, Andrew K. L. Lim†‡, A. Paul Alivisatos†‡ & Paul L. McEuen*‡

* *Department of Physics and* † *Department of Chemistry, University of California, Berkeley, California 94720, USA*
‡ *Molecular Design Institute, Lawrence Berkeley National Laboratory, Berkeley, California 94720, USA*

The techniques of colloidal chemistry permit the routine creation of semiconductor nanocrystals[1,2] whose dimensions are much smaller than those that can be realized using lithographic techniques[3–6]. The sizes of such nanocrystals can be varied systematically to study quantum size effects or to make novel electronic or optical materials with tailored properties[7–9]. Preliminary studies of both the electrical[10–13] and optical properties[14–16] of individual nanocrystals have been performed recently. These studies show clearly that a single excess charge on a nanocrystal can markedly influence its properties. Here we present measurements of electrical transport in a single-electron transistor made from a colloidal nanocrystal of cadmium selenide. This device structure enables the number of charge carriers on the nanocrystal to be tuned directly, and so permits the measurement of the energy required for adding successive charge carriers. Such measurements are invaluable in understanding the energy-level spectra of small electronic systems, as has been shown by similar studies of lithographically patterned quantum dots[3–6] and small metallic grains[17].

Fig. 1a shows an idealized diagram of the device. CdSe nanocrystals 5.5 nm in diameter[18,19] are bound to two closely spaced gold leads by bifunctional linker molecules[20,21]. The leads are fabricated on a degenerately doped silicon wafer, which is then used as a gate to tune the charge state of the nanocrystal under study. Figure 1b shows a field-emission scanning electron micrograph of a completed device. A number of nanocrystals seem to be in the ~5 nm gap between the electrodes.

Most devices, including the particular junction shown in Fig. 1b, have immeasurably high impedance ($R > 100\ \mathrm{G\Omega}$). Only about 1 in 20 have a measurable conductance, typically in the range 10 MΩ to 1 GΩ. Devices of this type typically behave as though transport is occurring through a single nanocrystal[11], as we demonstrate below. This may initially seem surprising, as Fig. 1b indicates that the number of nanocrystals in the junction region is quite large. However, tunnelling through the linker molecules has an exponential decay length of less than 1 Å (refs 11, 20, 22). As a result, only a well-placed nanocrystal (within 2 nm of each lead) can contribute to conduction.

Figure 2 shows the linear response conductance, G, of a device measured at $T = 4.2$ K as a function of the gate voltage, V_g, applied to the substrate. As the gate bias is raised, the conductance grows to a peak and then declines to zero again. In the insets to Fig. 2 the current, I, flowing through the nanocrystal is plotted as a function of the voltage, V, applied between the two leads at two fixed values of V_g. The I–V taken at a V_g away from the linear response peak shows

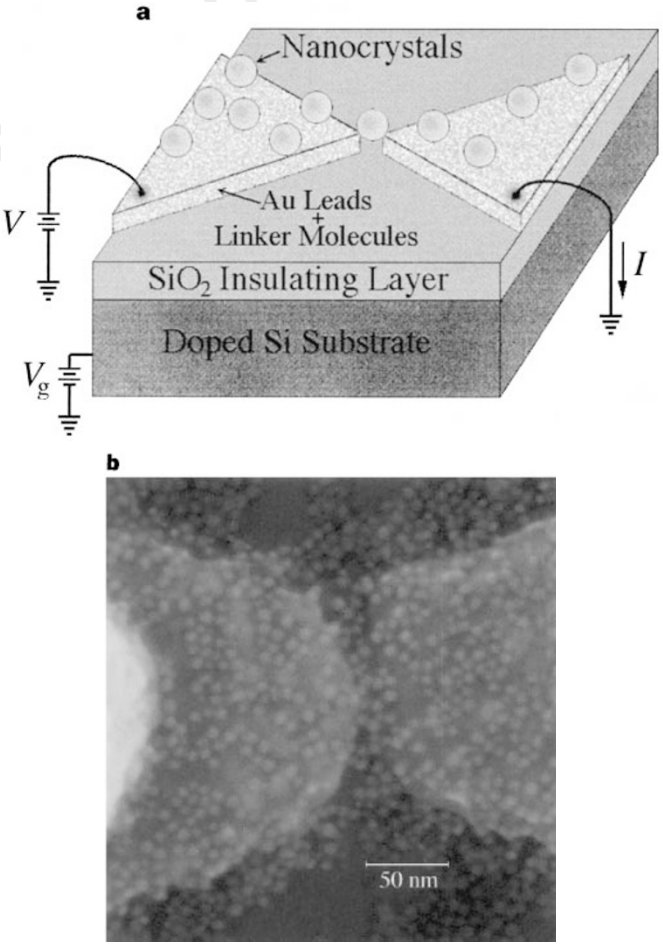

Figure 1 a, Diagram of the device. Nanocrystals sit on top of two closely spaced leads. Transport measurements probe the nanocrystal that best bridges the gap between the leads. The electrochemical potential of this nanocrystal can be tuned by applying a gate voltage to the substrate. **b**, Field-emission scanning electron micrograph of a set of 13-nm-thick leads separated by a ~10 nm gap onto which CdSe nanocrystals 5.5 nm in diameter have been deposited. A combination of optical and electron-beam lithography coupled with shadow evaporation is used to define these leads. The leads are patterned on a degenerately doped wafer on which an oxide barrier 53 nm thick has been grown. The nanocrystals have a mean diameter of 5.5 nm and a 5% coefficient of variation and are attached to the leads with 1,6-hexanedithiol. One end of these linear dithiol molecules binds to gold leads and the other binds to the nanocrystals to form a 1.2-nm-thick insulating barrier. Further fabrication details are described in ref. 11.

a suppressed conductance at small V whereas the I–V characteristic taken at the centre of the peak has a finite linear conductance for small V. Figure 3 shows a map of the differential conductance of the device, plotted as a grey scale, as a function of both V and V_g.

These measurements can be understood by using ideas borrowed from studies of lithographically patterned dots[3,5,6]. The conductance peak in Fig. 2 is a Coulomb oscillation. The suppressed conductance on each side of the peak is a consequence of the finite energy required to add (remove) an electron to (from) the nanocrystal in its ground state. This energy is analogous to the electron affinity (ionization energy) of a molecule. The peak occurs when the two charge states of the nanocrystal have the same total (including electrostatic) energy and an extra electron can therefore hop on and off the nanocrystal at no energy cost. The maximum size of the gap in the I–V curves away from the peak provides a measure of the addition (removal) energy for electrons, as we discuss below.

Figure 4a is a schematic energy level diagram of the nanocrystal with N electrons at a gate voltage midway between two Coulomb oscillations. The electrochemical potential for adding the $(N+1)$th electron to the nanocrystal is denoted μ_{N+1}. The energy difference Δ_{N+1} between μ_{N+1} and μ_N is referred to as the addition energy. In the simplest model, referred to as the Coulomb blockade model[6], the addition energy is given by:

$$\Delta_{N+1} = \mu_{N+1} - \mu_N = U + \Delta E$$

where U is the Coulomb interaction energy between any two electrons on the nanocrystal and $\Delta E = E_{N+1} - E_N$ is the energy-level spacing to the next unoccupied single-particle eigenstate.

When the linear-response conductance is zero, a finite V can adjust the Fermi energies of the leads relative to the nanocrystal to add or remove an electron to or from the nanocrystal. The Fermi level to the left lead, equal to $\sim eV$, can either rise above μ_{N+1} or fall below μ_N, allowing current to flow. The range of V for which the conduction is zero is referred to as the Coulomb gap. This gap varies as a function of V_g. The maximum size of the Coulomb gap for N electrons on the nanocrystal, in other words the maximum voltage V that can be applied without current flow, is a direct measurement of the addition energy Δ_{N+1} for the next electron. This is illustrated in Fig. 4b.

The evolution of the Coulomb gap with V_g can be seen in Fig. 3a and b, where the differential conductance dI/dV is plotted as a function of both V_g and V. The Coulomb gap produces the light-coloured diamond-shaped regions in these figures. The Coulomb gap is zero at a Coulomb oscillation; it grows to a maximum size approximately halfway between two oscillations, and then decreases again to zero at the next Coulomb oscillation. Figure 3c shows a schematic evolution of the Coulomb gap, along with the inferred addition energies, Δ_N, for successive electrons. These energies range from ~15 to 30 meV.

Similar, although less complete, results have also been obtained in two other gated samples. In addition, I–V measurements on eight other samples without a gate have been performed, some of which have been presented previously[11]. The addition energies determined for these samples are typically between 30 and 60 meV.

In the Coulomb blockage model, the addition energy for adding successive carriers is $U + \Delta E$. A straightforward electrostatic estimate for U, including the screening effects of the metallic leads, yields $U \sim 50$ meV for a 5.5-nm-diameter metallic sphere[11]. The level spacing, ΔE, depends on the type of charge carriers and is predicted to be ~100 meV for electrons and ~10 meV for holes[23]. The measured values of 15–60 meV for the addition energies are thus consistent with, but somewhat smaller than, expectations (~50–60 meV) for individual holes on a CdSe nanocrystal.

We now address an intriguing aspect of the data. Note that on the

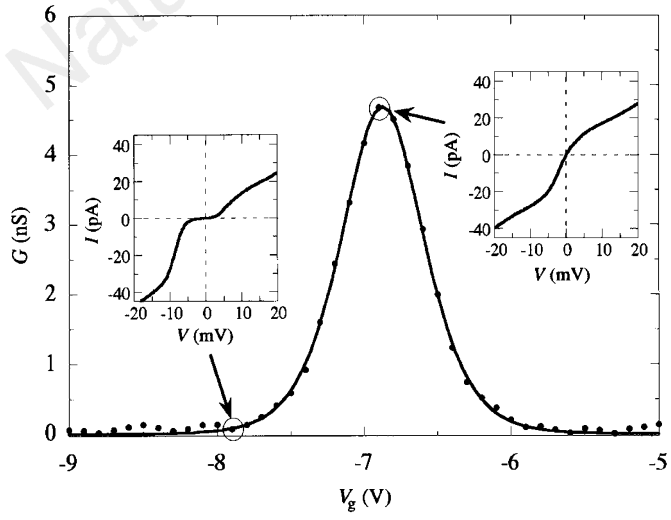

Figure 2 Conductance, G, plotted against gate voltage, V_g, for a single-nanocrystal transistor measured at $T = 4.2$ K. The conductance shows a peak when the charge state of the nanocrystal changes by one electron. The dots are the measured values; the solid curve is a fit to the data by using the standard Coulomb blockade model[6] with a temperature $T = 5$ K. Insets: I–V characteristics measured at the gate voltages indicated.

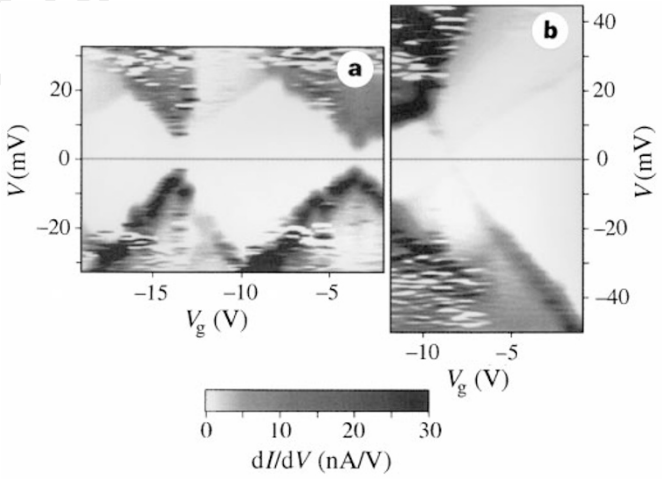

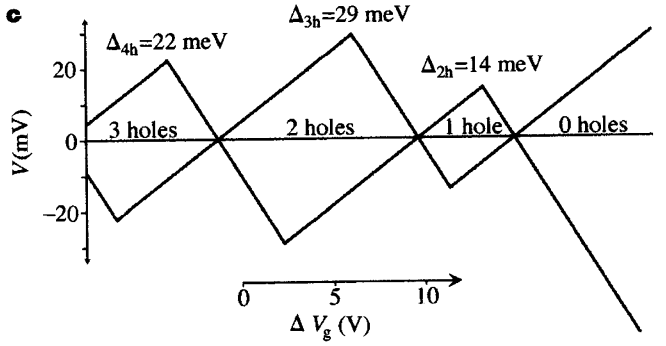

Figure 3 a, **b**, Composite grey-scale plots of the differential conductance dI/dV of a CdSe nanocrystal plotted as a function of both V_g and V. The white diamond-shaped regions correspond to the Coulomb gap. During the course of acquiring these data, several 'switches' occurred where the entire characteristic shifted along the V_g axis. These switches are ubiquitous in Coulomb blockade measurements and are thought to result from sudden changes in the local electrostatic environment. One such change occurred between the acquisition of **a** and **b**. During the acquisition of **a**, two smaller shifts occurred. To account for this, some parts of the data have been translated along the V_g axis. **c**, A schematic illustration of the data from **a** and **b**, indicating the inferred number of holes on the nanocrystal as a function of V_g and the addition energy for successive holes.

right side of Fig. 3 the Coulomb gap continues to grow with increasingly positive V_g. For even larger gate voltages than shown in the figure (up to 40 V) the Coulomb gap exceeds 150 mV and there is no evidence for any more Coulomb oscillations.

This behaviour can be understood if electrons are being added to the valence band of the nanocrystal with increasingly positive V_g. In this case, for some sufficiently positive V_g, every state in the valence band is filled, and the next extended state of the nanocrystal lies in the conductance band, $2eV$ higher in energy. In this interpretation, the large gap at positive V_g corresponds to a completely filled valence band. Starting on the right side of Fig. 3 and decreasing V_g, the first Coulomb oscillation of Fig. 3 then corresponds to the removal of the first electron from, or alternatively the addition of the first hole to, the valence band. A further decrease in V_g adds additional holes. The addition energies for the second, third and fourth holes are $\Delta_2 = 14 \pm 2$ meV, $\Delta_3 = 29 \pm 3$ meV and $\Delta_4 = 22 \pm 2$ meV, as is indicated in Fig. 3c.

Note that in the Coulomb blockade model, the energy Δ_2, for adding the second hole to the nanocrystal is simply the Coulomb interaction, U, between holes, as the lowest-lying hole state is doubly degenerate. The energy, Δ_3, for adding the third hole, in contrast, is $U + \Delta E$, where ΔE is the difference between the ground and first excited single-particle state. The addition energy for the fourth hole, Δ_4, is again U because the first excited state is also doubly degenerate. The results given above are somewhat consistent with this scheme: for example, Δ_3, predicted to be $U + \Delta E$, is greater than Δ_2, which is predicted to be U.

Nevertheless, discrepancies remain. The energy for adding the second hole, $\Delta_2 = 14$ meV, is significantly smaller than the values of $U \sim 50$ mV obtained from simple electrostatic estimates or from measurements of other samples. In addition, the measured Δ_4 is greater than Δ_2, whereas in the Coulomb blockade model they should be the same. The origin of these differences remains unclear, although the effects of exchange and correlations are expected to be important for these few-hole systems. We also emphasize that the large gap at positive V_g has been seen in only one device. To confirm that this gap is associated with a filled valence band and to verify the inferred hole addition energies, it will be necessary to repeat these measurements on other samples.

This work represents a new type of spectroscopy for single nanocrystals. Unlike optical measurements, where electron–hole pairs are created, these measurements probe the energy for adding a single type of charge carrier. We hope that these results will stimulate new calculations of the hole addition energies for a CdSe nanocrystal that include the effects of exchange, correlations, and screening by the metallic electrodes. Future measurements will investigate how the ground-state and excited-state properties vary with the size, shape and composition of nanocrystals as well as with the composition of the leads. □

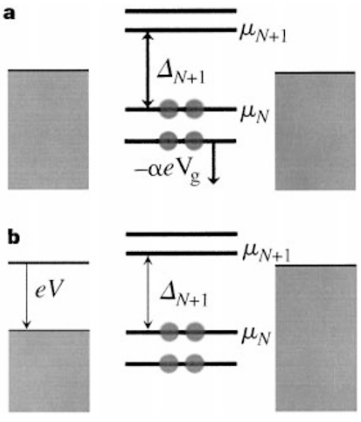

Figure 4 a, Energy-level diagram for a nanocrystal with N electrons at a gate voltage midway between two Coulomb oscillations. The electrochemical potential of the N-electron nanocrystal is denoted μ_N, and the electrochemical potential of the $(N + 1)$-electron nanocrystal is denoted μ_{N+1}. **b**, The application of a finite bias, V, can overcome the Coulomb gap. The maximal V applied before conduction occurs is equal to the addition energy, Δ_{N+1} for the $(N + 1)$th electron.

Received 9 June; accepted 31 July 1997.

1. Brus, L. Quantum crystallites and nonlinear optics. *Appl. Phys. A* **53,** 465–474 (1991).
2. Alivisatos, A. P. Semiconductor clusters, nanocrystals, and quantum dots. *Science* **271,** 933–937 (1996).
3. Kastner, M. A. Artificial atoms. *Phys. Today* **46,** 24–31 (1993).
4. Ashoori, R. C. Electrons in artificial atoms. *Nature* **380,** 559 (1996).
5. Tarucha, S., Austing, D. G., Honda, T., van der Hage, R. J. & Kouwenhoven, L. P. Shell filling and spin effects in a few electron quantum dot. *Phys. Rev. Lett.* **77,** 3613–3616 (1996).
6. Kouwenhoven, L. P. & McEuen, P. L. in *Nanoscience and Technology* (ed. Timp, G.) (AIP Press, New York, in the press).
7. Colvin, V. L., Schlamp, M. C. & Alivisatos, A. P. Light-emitting diodes made from cadmium selenide nanocrystals and a semiconducting polymer. *Nature* **370,** 354–357 (1994).
8. Dabbousi, B. O., Bawendi, M. G., Onitsuka, O. & Rubner, M. F. Electroluminescence from CdSe quantum-dot/polymer composites. *Appl. Phys. Lett.* **66,** 1316–1318 (1995).
9. Greenham, N. C., Peng, X. & Alivisatos, A. P. Charge separation and transport in conjugated-polymer/semiconductor-nanocrystal composites studied by photoluminescence quenching and photoconductivity. *Phys. Rev. B* **54,** 17628–17637 (1996).
10. Alperson, B., Cohen, S., Rubinstein, I. & Hodes, G. Room-temperature conductance spectroscopy of CdSe quantum dots using a modified scanning force microscope. *Phys. Rev. B* **53,** 17017–17020 (1995).
11. Klein, D. L., McEuen, P. L., Bowen Katari, J. E. & Alivisatos, A. P. An approach to electrical studies of single nanocrystals. *Appl. Phys. Lett.* **68,** 2574–2576 (1996).
12. Andres, R. P. *et al.* Coulomb staircase at room temperature in a self-assembled molecular nanostructure. *Science* **272,** 1323–1325 (1996).
13. Sato, T. & Ahmed, H. Observation of a Coulomb staircase in electron transport through a molecularly linked chain of gold colloidal particles. *Appl. Phys. Lett.* **70,** 2579–2761 (1997).
14. Blanton, S. A., Dehestani, A., Lin, P. C. & Guyotsionnest, P. Photoluminescence of single semiconductor nanocrystallites by two-photon excitation microscopy. *Chem. Phys. Lett.* **229,** 317–322 (1994).
15. Empedocles, S. A., Norris, D. J. & Bawendi, M. G. Photoluminescence spectroscopy of single CdSe nanocrystallite quantum dot. *Phys. Rev. Lett.* **77,** 3873–3876 (1996).
16. Nirmal, M. *et al.* Fluorescence intermittency in single cadmium selenide nanocrystals. *Nature* **383,** 802–804 (1996).
17. Ralph, D. C., Black, C. T. & Tinkham, M. Gate-voltage studies of discrete electronic states in aluminum nanoparticles. *Phys. Rev. Lett.* **78,** 4087–4090 (1997).
18. Bowen-Katari, J. E., Colvin, V. L. & Alivisatos, A. P. X-ray photoelectron spectroscopy of CdSe nanocrystals with applications to studies of the nanocrystal surface. *J. Phys. Chem.* **98,** 4109–4117 (1994).
19. Murray, C. B., Norris, D. B. & Bawendi, M. G. Synthesis and characterization of nearly monodisperse CdE (E = S, SE, TE) semiconductor nanocrystals. *J. Am. Chem. Soc.* **115,** 8706–8715 (1993).
20. Porter, M. D., Bright, T. B., Allara, D. L. & Chidsey, C. E. D. Spontaneously organized molecular assemblies. IV. Structural characterization of n-alkyl thiol monolayers on gold by optical ellipsometry, infrared spectroscopy, and electrochemistry. *J. Am. Chem. Soc.* **109,** 3559–3568 (1987).
21. Bain, C. D. *et al.* Formation of monolayer films by the spontaneous assembly of organic thiols from solution onto gold. *J. Am. Chem. Soc.* **111,** 321–335 (1989).
22. Boulas, C., Davidovits, J. V., Rondelez, F. & Vuillamueme, D. Suppression of charge carrier tunneling through organic self-assembled monolayers. *Phys. Rev. Lett.* **76,** 4797–4800 (1996).
23. Ekimov, I. *et al.* Absorption and intensity-dependent photoluminescence measurements on CdSe quantum dots: assignment of the first electronic transitions. *J. Opt. Soc. Am.* **10,** 100–107 (1993).

Acknowledgements. This work was supported by the US Department of Energy and by the Office of Naval Research.

Correspondence and requests for materials should be addressed to P.L.M. (e-mail: mceuen@physics.berkekely.edu).

A tough SiAlON ceramic based on α-Si_3N_4 with a whisker-like microstructure

I-Wei Chen*† & Anatoly Rosenflanz*†

* *Department of Materials Science and Engineering, University of Michigan, Ann Arbor, Michigan 48109-2136, USA*

Silicon nitride (Si_3N_4) is a light, hard and strong engineering ceramic[1,2]. It can withstand harsh environments and support heavy loads at temperatures beyond those at which metals and polymers fail. It can also be manufactured reliably at a reasonable cost and in large quantities. There are two forms of silicon nitride[3]: α-Si_3N_4 and β-Si_3N_4. The former is harder, but only

† Present address: Department of Materials Science and Engineering, University of Pennsylvania, 3231 Walnut Street, Philadelphia, Pennsylvania 19104-6272, USA.